An engineering model for creeping flame spread over idealized electrical wires in microgravity

Alain Coimbra, Yutao Li, Augustin Guibaud, Jean-Marie Citerne, Guillaume Legros, Jean-Louis Consalvi

INSTITUT DE FRANCE
Académie des sciences

Comptes Rendus
Mécanique

Alain Coimbra, Yutao Li, Augustin Guibaud, Jean-Marie Citerne, Guillaume Legros and Jean-Louis Consalvi

An engineering model for creeping flame spread over idealized electrical wires in microgravity

Published online: 10 March 2023

https://doi.org/10.5802/crmeca.149

Part of Special Issue: Physical Science in Microgravity within the Thematic Group Fundamental and Applied Microgravity

Guest editors: Olga Budenkova (CNRS, Université Grenoble Alpes,Grenoble INP, SIMaP, 38000 Grenoble, France),
Catherine Colin (IMFT, Université de Toulouse, CNRS, INPT, UPS et GDR 2799 Micropesanteur Fondamentale et Appliquée) and Guillaume Legros (ICARE, CNRS UPR 3021, Univ. Orléans et GDR 2799 Micropesanteur Fondamentale et Appliquée)

Les Comptes Rendus. Mécanique *sont membres du Centre Mersenne pour l'édition scientifique ouverte*
www.centre-mersenne.org
e-ISSN : 1873-7234

Comptes Rendus
Mécanique
Published online: 10 March 2023
https://doi.org/10.5802/crmeca.149

Physical Science in Microgravity within the Thematic Group Fundamental and Applied Microgravity / *Sciences physiques en microgravité au sein du GDR Micropesanteur Fondamentale et Appliquée*

An engineering model for creeping flame spread over idealized electrical wires in microgravity

Alain Coimbra [a], Yutao Li [b], Augustin Guibaud [c], Jean-Marie Citerne [b], Guillaume Legros [d] and Jean-Louis Consalvi [*, a]

[a] Aix-Marseille Université, CNRS, IUSTI UMR 7343, 5 rue E. Fermi, 13013 Marseille, France

[b] Institut Jean le Rond d'Alembert/UMR CNRS 7190, Sorbonne Université, Paris F-75005, France

[c] Department of Civil, Environmental and Geomatic Engineering, University College London, London WC1 E6BT, UK

[d] ICARE/CNRS, 1C av. de la Recherche Scientifique, Orléans Cedex 1 45071, France

E-mails: alain.coimbra@univ-amu.fr (A. Coimbra), yutao.li@hotmail.com (Y. Li), a.guibaud@ucl.ac.uk (A. Guibaud), jean-marie.citerne@sorbonne-universite.fr (J.-M.. Citerne), guillaume.legros@cnrs-orleans.fr (G. Legros), jean-louis.consalvi@univ-amu.fr (J.-L. Consalvi)

Abstract. Flame spread over an insulated electrical wire is a major source of fire scenario in a space vehicle. In this work, an engineering model that predicts the creeping flame spread over cylindrical wires in microgravity is developed. The model is applied to interpret experimental data obtained in parabolic flights for wires composed by a 0.25 mm radius nickel-chromium (NiCr) metallic core coated by low-density polyethylene (LDPE) of different thicknesses ranging from 0.15 mm to 0.4 mm. The model relies on the assumption that, in the pyrolysis region, the NiCr and the LDPE are in thermal equilibrium. This assumption is supported by more detailed numerical simulations and the model reduces then to solving the heat transfer equations for both NiCr and LDPE in the pyrolysis region and in the region ahead of the flame front along with a simple degradation model for LDPE, an Oseen approximation of opposed oxidizer flow and an infinitely fast gas-phase chemistry. The flame spread rate (FSR) is controlled by two model parameters, which are measurable from intrinsic material and ambient gas properties: the convective flame heat flux transferred to the solid ahead from the flame front and the gaseous thermal heat length near the flame front. These parameters are then calibrated from experimental data for a given wire geometry and the calibrated model is validated against experimental data for other wire geometries and ambient conditions. The heat transfer mechanisms ahead of the pyrolysis front are investigated with a special emphasis on the LDPE thickness and the conductivity of the metallic core. In addition to NiCr, metallic cores of lower and higher conductivities are considered. The polymer is shown to be thermally thick for all tested wire geometries and core conductivities. The flame heat flux is found to dominate the heat transfer in the preheat zone where it applies. The core has

* Corresponding author.

nevertheless a significant impact in the heating of the LDPE with its contribution increasing with the core conductivity and when decreasing the LDPE thickness.

Keywords. Creeping flame spread, electrical wire, microgravity, low-density polyethylene, nickel-chromium core.

Published online: 10 March 2023

1. Introduction

In order to achieve the ambitious goals of manned deep space exploration in the near future, several safety issues aboard the spacecrafts must be resolved. Fire hazards in such confined environments are a threat to equipment integrity and even the safety of the astronauts. The main potential source of a fire in this situation is attributed to electrical malfunction. The insulation and jacket layers of wire and cable are made of plastic materials, which may release pyrolysis gases when heated by external sources or short-circuiting, supporting combustion. This common scenario of flame spread over polymer-coated electrical wires has motivated extensive research in both normal gravity [1–4] and microgravity [5–10].

Simplifying the in-flight configuration to a one dimensional academic problem, the analysis of steady state opposed flow flame spread over a vertical wire is key to understanding the flammability of solid fuels [11]. Flame spread over solid surfaces results from the heating process of the material ahead of the pyrolysis front. Heat transfers of multiple natures raise the unburnt solid from the ambient temperature up to the pyrolysis temperature at which the material starts to release gaseous fuel that is ignited by the flame, ensuring the spreading process [12]. The flame spread process can be viewed then as a series of piloted ignitions where the flame acts as both heating source and pilot [13].

Flame spread models and correlations have been proposed for steady-state opposed flame spread, denoted also as creeping flame spread [13]. Most notably, a model based on the heat balance ahead of the pyrolysis front in both thermally-thin and thick slabs has been proposed by de Ris [14]. In this approach, the heat transfer from the flame to the solid was obtained by solving the laminar boundary layer equation along with the infinitely fast gas-phase chemistry and Oseen approximations. The flame spread rate (FSR) could be then assessed and characterized based on measurable material and gas properties. It was nevertheless observed that this model largely overestimates the flame heat transfer and the corresponding FSR, owing to the assumption of infinitely fast kinetics, which is not satisfied at the flame leading edge. In this region, the relatively cold solid surface acts as a heat sink that produces local flame extinction, resulting in a complex flame attachment process [11].

In order to circumvent these difficulties and to provide an engineering analytical flame spread model, Delichatsios and co-workers reduced the flame heat transfer process to two properties, measurable from material and ambient gas properties, that characterize the creeping flame spread process: the convective heat flux per unit length, $E'_{gs,pr}$, from the flame to material near the pyrolysis front and the gaseous thermal length, L_g, generated by the opposed oxidizer flow [15]. In addition, they provide experimental methodology and methods for their determination. A heat balance equation and its corresponding methodology was first proposed for a flat burning surface [15], before being extended to cylindrical samples [16]. As compared to flat geometry, the cylindrical curvature was found to modify the heat balance by enhancing gas-to-surface heat transfer and by reducing the heated layer depth in the solid. This heat balance was also developed for a flat material undergoing a melting process [17].

A unique feature in the flame spread over electric wires is the presence of an inert, high thermal conductivity metallic core inside the flammable polymer coating. The presence of the

core is known to modify the heat transfer pattern, from the ignition, spread, extinction to the phase-change processes of the polymer insulation and emission of combustion products [4, 18]. It was shown that increasing the thermal conductivity of the core results in an increased FSR, but simultaneously increases the local extinction behavior due to increased heat losses in the the unburned zone [19]. This process is impacted however by several parameters, as the role of the metallic core as a heat sink or heat source is shown to be controlled by the wire material properties, geometry and ambient conditions, most of which are not well understood [4].

A detailed description of the heat transfer process in the case of a thermally-thin idealized electrical wire consisting of a metallic core and a LDPE coating has been provided by Konno et al. [20] and is displayed in Figure 1. The heat transfer to the virgin polymer upstream to the pyrolysis front is driven by both the flame heat flux and the heat transfer from the metallic core. As observed in the experiments of Guibaud et al. [21], the polymer is entirely consumed by the degradation process, leading to a diffusion flame that falls down to the bare wire at the trailing edge (See Figure 1). This induces a substantial heat flux from the flame to the bare wire, which is in turn conducted through the metallic core towards the pyrolysis zone, contributing in addition to the flame heat flux to pyrolyse the solid. A part of this flux is then transferred though the metallic core ahead of the pyrolysis zone.

The objective of this study is to predict creeping flame spread over idealized polymer coated metallic wires in microgravity. It will be shown how this complex heat transfer behaviour can be simplified if the pyrolysis can be treated as phase-change as assumed in the aforementioned heat balance flame spread models. An engineering heat balance flame spread model and an experimental procedure to determine the material properties characterizing the creeping flame spread over thin electrical wires are developed. The experiments made by Guibaud and co-workers on Nickel-Chrome (Nicr)/Low Density PolyEthylene (LDPE) electrical wires will be considered to determine these parameters and validate the model [21]. These experiments and assumptions for characterizing steady flame spread are described in Section 2. The flame spread model, governing equations and considered material and gas-phase properties will be subsequenty presented in Section 3. The results will be discussed in Section 4. The calibration of the model parameters is presented and validated against experimental data. Then, a study of the heat transfer mechanisms in the wire is discussed. Finally, Section 5 will be devoted to the conclusions and perspectives of this study.

2. Experimental methodology

The experimental procedure used to obtain the flame spread rate is briefly described in this section. Experiments in microgravity are conducted on the Detection of Ignition And Mitigation Onboard for Non-Damaged Sapcecrafts (DIAMONDS) rig, which is extensively described in Ref. [8, 22]. DIAMONDS was installed aboard the Novespace A310 ZeroG airplane, a facility that specifically operates parabolic flights. Every parabola provides a 22 s long sequence of microgravity with an accuracy level of $5{\cdot}10^{-2}$ g_0 ($g_0 = 9.81$ m/s^2). The experimental setup consists of a cylindrical combustion chamber with an inner diameter of 190 mm, where a laminar O_2/N_2 oxidizer flow can be established with a direction from the bottom to the top of the chamber. The flow conditions can be controlled with the oxygen content in volume fraction from 0-21%, the pressure from 50.7-121.6kPa and the flow velocity from 0-300 mm/s. The samples are cylindrical wires of length 150 mm, composed of a NiCr core coated by LDPE insulation. They were placed along the central axis of the chamber and parallel to the flow direction. LDPE has been used as coating of laboratory wires as an international target configuration to investigate flammability properties of electrical cables in both normal and microgravity conditions [4, 5, 23]. In these experiments, three core-to-wire radius ratios, R_c/R_s were tested: (i) 0.25/0.4 (Type#1),

(ii) 0.25/0.55 (Type#2) and (iii) 0.25/0.65 (Type#3), as summarized in Table 1. The core radius was kept unchanged and the LDPE thickness, δ_s, was varied. The cross sections area ratio, A_c/A_s, of Type#1 is about 2 and 2.63 times larger than those of Type#2 and Type#3, respectively. The samples were ignited using a hot Kanthal wire located at its upper end to initiate an opposed-flow flame spread.

Table 1. Configurations of NiCr core and LDPE insulations

Type	R_c (mm)	R_s (mm)	δ_s (mm)	A_c/A_s
I	0.25	0.40	0.15	0.391
II	0.25	0.55	0.30	0.206
III	0.25	0.65	0.40	0.148

All experiments are recorded in using a JAI AT-140CL digital tri-CCD camera, equipped with a telecentric lens to restrict the light collection to beams parallel to the optical axis. A controlled uniform LED backlight is set on and off alternatively during the images acquisition in order to track the morphology of flame and LDPE droplet. Images are captured with a frame rate of 39.06fps over a 512x1396 pixels^2 CCD array in the red, green and blue spectral bans with a resolution of 72.6 μm, which can provide an entire view during the flame spread. FSR is determined by tracking the flame front using image without backlighting processing once a steady flame spread is reached. A detailed description can be found in Ref. [24]. According to the images with backlighting, the spreading over LDPE is characterized by the formation of a molten droplet whose, for the conditions investigated in the present study, volume increases first before reaching a steady value. The flame is assumed to spread at a steady rate once the dimensions of the molten insulation droplet, the visible flame length, and the rate of the flame front displacement reach a steady state value.

3. Flame spread model

3.1. *Model assumptions*

The model considers a flame spreading at a steady rate over a thin electrical wire composed by a metal core of radius R_c and a polymer coating of radius R_s. During steady-spread rate, the wire can be decomposed into four regions as illustrated in Figure 1. The region directly ahead of the pyrolysis front is referred to as the preheat zone and involves the heat transfer between the flame, the metallic core and the LDPE. This region is proceeded by the unburnt zone where the heating process is manly driven by conduction through the metallic core. The pyrolysis zone is located downstream the pyrolysis front followed by a bare metallic core as the polymer is completely burnt. The following assumptions are introduced:

(1) The polymer melting and the pyrolysis processes behave as phase changes occurring at temperatures $T_s = T_m$ and $T_s = T_p$, respectively.
(2) The polymer can expand or contract in the $r-$ direction.
(3) The pyrolysis front corresponds to the location at time t, $z_p(t)$, where the wire surface temperature reaches the pyrolysis temperature, T_p.
(4) In the pyrolyzing zone, the temperature of the polymer layer is maintained constant to $T = T_p$.
(5) In the pyrolyzing region, the metal core and the polymer layer become rapidly in thermal equilibrium. This assumption implies that the heat flux conducted from the bare metal

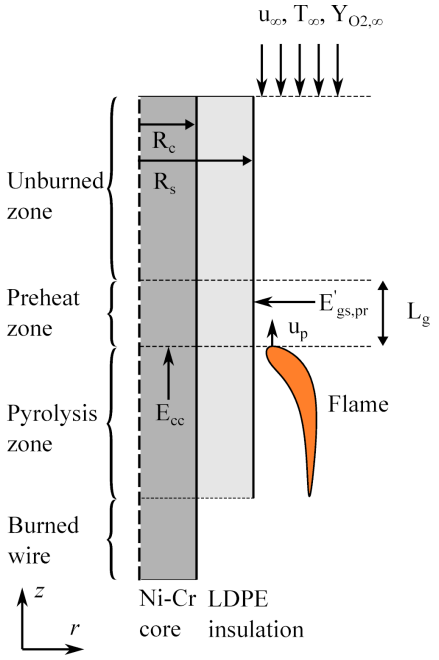

Figure 1. Scheme of the engineering flame spread model (not in scale). The distinction between the preheat and unburned zones is reproduced from the works of Konno et al. [20].

core toward the pyrolyzing region is completely transferred to the pyrolyzing polymer. Therefore, it does not affect the heat balance in the preheat region, and, in turn, the flame spread. The validity of this assumption has been assessed by using the CFD model described in detail in Refs. [21, 23, 25]. During these simulations, it was assumed that the pyrolyzing LDPE is at T_p, consistently with the assumption (4). The results are reported in Figure 2 that shows the evolution along the wire axis of the temperatures inside the metal core and LPDE for a simulation considering a LPDE/NiCr of Type#2 (see Table 1), an oxidizer composed of 21%-O_2/ 79%-N_2 flowing at a velocity of 150 mm/s and a pressure of 101 kPa. The same behavior has been observed for the other wire geometries and ambient conditions. The location z =0 corresponds to the pyrolysis front and the negative values of z to the region ahead of the pyrolysis front. The pyrolysing region is located between $z = 0$ and $z \approx 0.008$ m followed by the bare NiCr for $z > 0.008$ m. Figure 2 shows that the NiCr temperature reaches a peak at the location where the flame falls down to the bare metal core. This temperature decreases downstream and upstream the peak due to thermal diffusion. In the pyrolyzing region, it reaches rapidly the pyrolysis temperature, demonstrating that the assumption of thermal equilibrium between the LDPE and the NiCr is satisfied provided that assumption (4) holds.

(6) In the preheat zone, the radiative flux from the flame is balanced by the heat flux re-radiated by the solid surface. This assumption is sustained by numerical simulations [21, 23, 25].

(7) The opposed flow is modelled as an Oseen flow with a vertically uniform velocity, u_∞, parallel to the wire axis.

(8) The combustion kinetics is assumed to be infinitely fast with $F(kg) + s\ O_2 \rightarrow (1+s)Pr$.

(9) The cylindrical curvature enhances the convective heat transfer from the flame to the solid as compared to a flat slab and a corrective factor is introduced to account for this

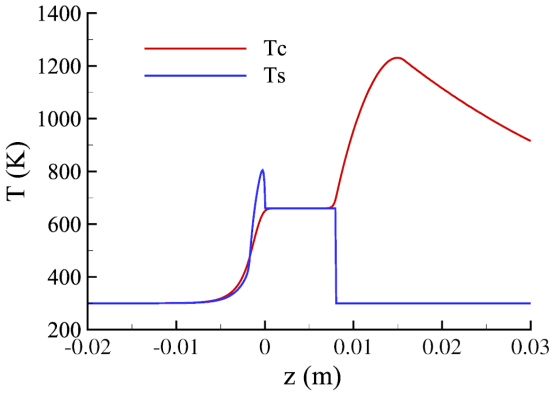

Figure 2. Evolution of LDPE, T_s, and NiCr, T_c, temperatures along the wire axis.

enhancement [16]. The convective heat power transferred from the flame to the polymer in the preheat region, $E_{gs,pr}$, can be estimated by using assumptions (6) to (8) [15, 16]:

$$E_{gs,pr} = 2\pi R_s \dot{q}''_{fl,c} L_g = 2\pi R_s E'_{gs,pr}. \tag{1}$$

In Eq. (1), L_g represents a gas-phase thermal diffusion length, i.e. the length over which the flame heat flux is applied. It is given by:

$$L_g = \frac{\alpha_g}{u_\infty} = \frac{k_g}{\rho_g c_g u_\infty}, \tag{2}$$

and $\dot{q}''_{fl,c}$ is the convective heat flux transferred from the flame to the solid. The diffusivity α is obtained from the conductivity, k_g, density, ρ_g, and heat capacity, c_g with the subscript g referring to gas properties. $E'_{gs,pr}$ is expressed as:

$$E'_{gs,pr} = \underbrace{\frac{\sqrt{\pi}\frac{L_g}{R_s}}{\ln\left(1+\sqrt{\pi}L_l/R_s\right)}}_{\mathrm{C}} \times \underbrace{k_g \frac{\left[B - r_f\right] L_v}{c_g}}_{E'_{gs,pr,flat}}. \tag{3}$$

$B = [Y_{O2,\infty}\Delta h_c/s - c_g(T_p - T_\infty)]/L_v$ is the mass transfer number, L_v the latent heat of gaseification, Δh_c the heat of combustion and $r_f = Y_{O2,\infty}/s$ the mass fuel-to-air ratio. $E'_{gs,pr}$ is composed of two contributions: the heat flux estimated for a flat slab, $E'_{gs,pr,flat}$, and a corrective factor to extend it to the cylindrical geometry, C. As discussed in the literature [15], the estimation of $E'_{gs,pr,flat}$ from the infinitely fast kinetics assumption leads to an overestimation of the heat flux from the flame to the unpyrolyzed polymer. For a given oxidizer composition, this property will be estimated from experiments for the Type#2 wire under a pressure of 101 kPa and will be applied to other wire and ambient conditions. The underlying assumption is:

(10) $E'_{gs,pr,flat}$ depends only of the oxygen concentration in the oxidizer, X_{O2} and, as a consequence, does not depend on the oxidizer flow rate, pressure, and wire geometry whose effects are captured through C and L_g.

The assumptions that the polymer pyrolysis can be assimilated to a vaporization process at constant pyrolysis temperature, T_p, (assumptions (1) and (3)) are the basis of the original formulations of the De Ris and Delichatsios flame spread models [14–16, 26] that serve as

strating point for the present study. However, they require further comments. First, analysis of the pyrolysis process of LDPE shows that it is more complex than a simple phase change [27]. Second, metallic core temperature measurements [28] have revealed that the metal core temperature does not exhibit the constant temperature behavior observed in Figure 2 in the pyrolysis region but increases continuously up to the peak. This suggests that the assumption of constant pyrolysis temperature in the polymer is questionable (see assumption (5)) and needs to be investigated in future works.

3.2. *Governing equations*

Based on the aforementioned assumptions, the axi-symmetric heat transfer equations and the corresponding boundary conditions for the LDPE coating and the NiCr core are given below. The assumption (3) defines the pyrolysis front as $z_p(t) = \underset{z}{max}\left(z|_{T_{s(R_s,z,t)=T_p}}\right)$ and the flame spread rate as:

$$u_p = \frac{dz_p(t)}{dt}. \tag{4}$$

The assumption (5) allows to simplify the problem by ignoring the heat flux transferred from the bare NiCr to the preheat zone and by reducing the computational domain to the pyrolysing zone, located for $z_p(t) - L_p \leq z \leq z_p(t)$, and the zone located ahead of the pyrolysis zone, $z > z_p(t)$, including the preheat zone and the unburned zone (see Figure 1). The pyrolysis length, L_p is assumed to be of 10 mm in accordance with experimental observations [29].

- For the LDPE: $R_c \leq r \leq R_s$
  - For $z \leq z_p(t)$:

$$T_s(r,z,t) = T_p \tag{5a}$$

  - For $z > z_p(t)$:

$$\frac{\partial \rho_s h_s}{\partial t} = \frac{1}{r}\frac{\partial}{\partial r}\left(r k_s \frac{\partial T_s}{\partial r}\right) + \frac{\partial}{\partial z}\left(k_s \frac{\partial T_s}{\partial z}\right) + \frac{1}{r}\frac{\partial}{\partial r}\left[\left(\int_{R_c}^{r} \frac{1}{\rho_s}\frac{\partial \rho_s}{\partial t} r dr\right)\rho_s h_s\right] \tag{5b}$$

for $T_s < T_m$ and $T_s > T_m$

$$0 = \frac{1}{r}\frac{\partial}{\partial r}\left(r k_s \frac{\partial T_s}{\partial r}\right) + \frac{\partial}{\partial z}\left(k_s \frac{\partial T_s}{\partial z}\right) - \dot{m}'''_m L_m \tag{5c}$$

for $T_s = T_m$ where $h_s = \int_0^{T_s} c_s dT$.
The third term in the right-hand side of Eq. (5b) represents the heat transfer associated with contraction or expansion of the material object. Equation (5c) describes the melting process.
The following boundary conditions are applied:

$$k_s \frac{\partial T_s}{\partial r} = \dot{q}''_{fl,c} \tag{6a}$$

For $r = R_s$ and $z_p \leq z \leq z_p + L_g$;

$$k_s \frac{\partial T_s}{\partial r} = h(T_\infty - T_s) \tag{6b}$$

For $r = R_s$ and $z \geq z_p + L_g$;

$$k_s \frac{\partial T_s}{\partial r} = k_c \frac{\partial T_c}{\partial r} \tag{6c}$$

For $r = R_c$ and $\forall\ z$;

$$\frac{\partial T_s}{\partial z} = 0 \tag{6d}$$

For $z \to \infty$;

$$T_s = T_p \tag{6e}$$

For $z < z_p - L_p$.
The convective coefficient h is computed as $h = k_g Nu/2R_s$, with $Nu = 0.32 + 0.155Re^{0.5}$ [30]. $Re = \rho_g u_\infty R_s/\mu_g$ is the Reynolds number with μ_g the kinematic viscosity.
The following initial conditions are also considered:

$$T_s(r, z, t = 0) = T_p \tag{7a}$$

For $z \leq z_p(t = 0)$;

$$T_s(r, z, t = 0) = T_\infty \tag{7b}$$

For $z > z_p(t = 0)$;

- For the NiCr: $0 \leq r \leq R_c$

$$\rho_c c_c \frac{\partial T_c}{\partial t} = \frac{1}{r}\frac{\partial}{\partial r}\left(r k_c \frac{\partial T_c}{\partial r}\right) + \frac{\partial}{\partial z}\left(k_c \frac{\partial T_c}{\partial z}\right) \tag{8}$$

The following boundary conditions are applied:

$$k_s \frac{\partial T_s}{\partial r} = k_c \frac{\partial T_c}{\partial r} \tag{9a}$$

For $r = R_c$ and $\forall\ z$;

$$\frac{\partial T_c}{\partial z} = 0 \tag{9b}$$

For $z \to \infty$;

$$\frac{\partial T_c}{\partial z} = 0 \tag{9c}$$

For $z = z_p - L_p$ and $\forall\ r$;
The initial condition is also applied:

$$T_c(r, z, t = 0) = T_\infty. \tag{10}$$

The heat transfer equations for the polymer and the metal core were solved in a coupled manner by using the finite volume method [31], a first-order backward Euler scheme for time integration and a second-order centered scheme for diffusion terms. The heat conductivity at the interface between LDPE and NiCr was computed with the harmonic mean to handle the large differences in conductivity between NiCr and LDPE [31].

A steady state flame front propagation was achieved approximately 1 s after the beginning of the simulations for all the wire geometries and ambient conditions, and an interval of $\Delta t = 1$ s between $t = 2$ and $t = 3$ s was used to capture the average spread rate from Eq. (4). A time step $\Delta t = 5.0 \times 10^{-5}$ s is used in all configurations. Multiplying or dividing this value by a factor of 10 was found to provide minor changes on the results. The spatial discretization is uniform, with a cell sizing of $\Delta z = 0.03$ mm and $\Delta r = 0.04$ mm. Multiplying or dividing these values by a factor of 2 was found to provide minor changes on the results.

3.3. *Material and gas phase properties*

The heat capacity, the melting temperature and the heat of melting of LPDE were obtained from differential scanning calorimetry. The evolution of the LDPE density with temperature was taken from literature [32] and it has been checked that the literature values at room temperature are equal to those measured in our experiments. The thermal conductivity of LPDE was measured using the transient line source method. These data are given in Table 2 for the LDPE and NiCr. The gas-phase density, heat capacity and conductivity are evaluated by assuming that the gas is air and by using a temperature evaluated as the average between the adiabatic flame temperature of ethylene in the investigated conditions and the ambient temperature.

Table 2. Thermal properties of the LDPE and Nickel-Chrome

Property	LDPE	NiCr
Density (kg/m^3)	$\rho_s = 948.2$ for $T_\infty < T_s < T_m$	$\rho_c = 8670$
	$\rho_s = 948.2 - 0.94(T_s - T_\infty)$ for $T_m < T_s < T_p$	$\rho_c = 8670$
Heat capacity (J/kg/K)	$c_s = 0.2T^2 - 105.7T + 15773$ for $T_\infty < T_s < T_m$	$c_c = 440$
	$c_s = 3.4T + 1228.3$ for $T_m < T_s < T_p$	$c_c = 440$
Thermal conductivity	$k_v = 0.38$	$k_c = 17.4$
(W/m/K)	$k_m = 0.45$	$k_c = 17.4$
Heat of melting (J/kg)	$L_m = 101000$	—
Melting temperature (K)	$T_m = 384$	—
Pyrolysis temperature (K)	$T_p = 690$ [28]	—

4. Results and Discussion

4.1. *Calibration of the model parameters*

As previously discussed in the model assumption (9), the infinitely fast kinetics assumption led to a systematic overestimation of the heat flux transferred from the flame to the unpyrolyzed polymer [15]. A calibration procedure is performed to estimate the model parameters L_g and $E'_{gs,pr,flat}$. L_g is determined from its definition (Eq. (2)) and $E'_{gs,pr,flat}$ is calibrated by assuming that the geometry effects are modelled through the geometric correction C and the effects of the oxidizer flow rate and ambient pressure are captured solely through L_g. A consequence is that $E'_{gs,pr,flat}$ is expected to depend only on the oxygen concentration in the oxidizer, X_{O2}.

The calibration procedure consists in fitting the experimental spread rate for the Type#2 wire, a pressure of 101 kPa and an inflow velocity of 150 mm/s. The fitted values are reported in Table 3. As expected, $E'_{gs,pr,flat}$ increases with X_{O2}. It can be also observed that the fitted values represent 30% of the theoretical value given by Eq. (3) whatever X_{O2}. The quality of the fit is demonstrated in Figure 3.

4.2. *Flame spread rate*

The model along with the calibrated values of $E'_{gs,pr,flat}$ is applied to the other wire geometries and ambient pressures. Figure 4 shows the predicted FSR by the present model (referred to as Num. in the legend) as a function of X_{O2} for the Type#1, Type#2 and Type#3 wires. As expected from experimental observations in microgravity for electrical wires [20, 33], the FSR increases

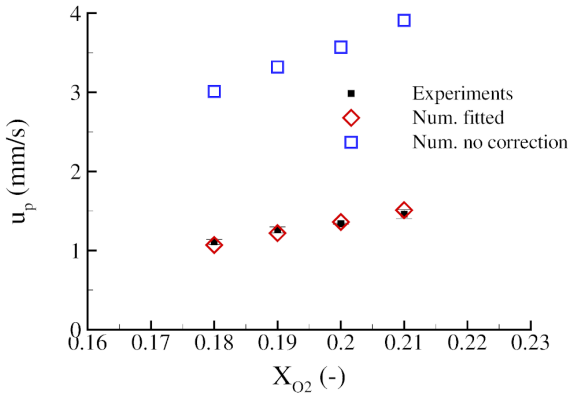

Figure 3. Spread rate as a function of X_{O2} for the Type#2 wire, an oxidizer velocity of 150 mm/s and a pressure of 101 kPa. The blue symbols represent the spread rate computed by using Eq. (3) whereas the red symbols represent that computed with the fitted $E'_{gs,pr,flat}$.

Table 3. Values of $E'_{gs,pr,flat}$ for the different values of X_{O2}.

X_{O2}	0.18	0.19	0.20	0.21
$\left[E'_{(gs,pr,flat)}\right]_{Calibrated}$ (W/m)	17.66	20.14	22.45	25.12
$\frac{\left[E'_{(gs,pr,flat)}\right]_{Calibrated}}{\left[E'_{(gs,pr,flat)}\right]_{Theoretical}}$	0.30	0.30	0.30	0.30

with X_{O2} for all the cases owing to an increase in flame temperature, which results in an increase of the flame heat flux transferred to the solid surface. This behavior is well captured by the model. The effect of wire geometry on the FSR is also well reproduced by the model. For a given X_{O2}, decreasing the wire diameter leads to an increase in the flame heat flux and, in turn, an increase in the FSR. This behavior was also observed in experiments involving black LDPE-coated copper wires [28].

Figure 4 compares also the experiments and the present predictions with the classical opposed-flow flame spread model proposed by Fernandez-Pello [13] and extended to cylindrical geometry in Ref. [34]. This model is referred to as CFP in Fig. 4 and ignores the heat transfer contribution of the metallic core. The flame spread velocity is given by:

$$u_p = 2C\frac{l_h\left(\dot{q}''_{fl,c}+\dot{q}''_{fl,r}-\dot{q}''_{rr}\right)}{\rho_s R_s\left[c_s(T_m-T_\infty)+L_m+c_s(T_p-T_m)\right]}-\text{func}\,(Da) \tag{11}$$

where Da is the Damkohler number and l_h is the solid heated length upstream of the flame front, taken equal to L_g to be consistent with our model. Da effects are neglected in accordance with the assumption of flame spread in the thermal regime whereas assumption (6) implies that $\dot{q}''_{fl,r} \approx \dot{q}''_{rr}$. The model has been slightly modified to include the contribution of the melting process and ρ_s and c_s are evaluated from the correlations of Table 2 at $\overline{T} = (T_m + T_\infty)/2$ before the melting and at $\overline{T} = (T_p + T_m)/2$ after the melting. Under these assumptions, Eq. (11) reduces

to the flame spread model proposed by Delichatsios et al. [16, 17] for cylindrical samples over a solid undergoing a melting process:

$$u_p = 2\frac{\frac{\sqrt{\pi}\frac{L_g}{R_s}}{ln(1+\sqrt{\pi}L_g/R_s)} \times E'_{gs,pr,flat}}{\rho_s R_s \left[c_s(T_m - T_\infty) + L_m + c_s(T_p - T_m)\right]} \tag{12}$$

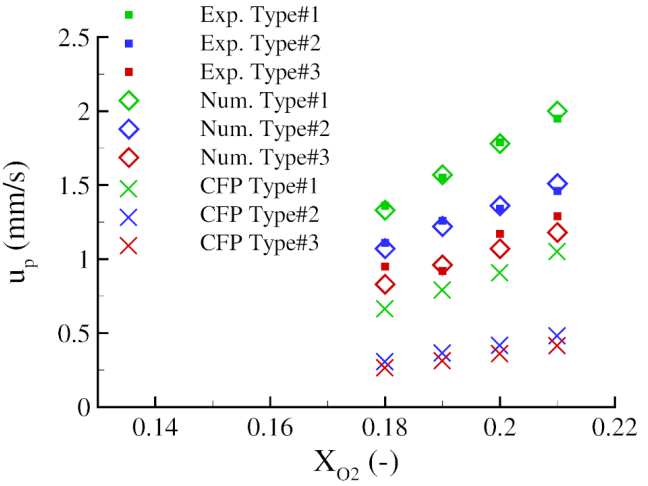

Figure 4. Spread rate as a function of X_{O2} for different wire geometries. The oxidizer velocity and the pressure are 150 mm/s and 101 kPa, respectively. The filled squared, the open diamonds and the crosses refer to the experiments, the present numerical model and the analytical model of Fernandez-Pello [13], respectively.

The CFM spread rates have been computed with the calibrated values of $E'_{gs,pr,flat}$ reported in Table 3. Figure 4 shows that the CFM model captures the trends, reproducing well the increase of u_p with X_{O2} and when decreasing the wire diameter. However, the spread rates predicted by the CFM model are significantly lower than those obtained experimentally, evidencing the contribution of the metallic core to the heat transfer to the LDPE.

The evolution of the FSR with X_{O2} is displayed for the Type#2 wire for different pressures in Figure 5. For a given oxygen concentration, the FSR slightly decreases while increasing the pressure due to an enhancement in the gas-phase density, ρ_g and, in turn, a reduction in L_g. This behaviour is well captured by the model. The good agreement between the model and the experiments for the different wire geometry and pressures supports the assumption (10).

4.3. *Heat transfer analysis*

Contours of temperature at steady spread rate for two LDPE thicknesses (Type#1 and Type#2 wires) are depicted in Figure 6. In this figure, the flame propagates from the bottom toward the top and the two heat fluxes as well as the preheat length, L_g, are indicated. The pyrolysis front is located at $z = 0$, and the vertical line shows the separation between the NiCr and LDPE.

The following conclusions may be drawn from analysis of Figure 6:

(1) The temperature gradients in the radial direction r observed in the LDPE coating in preheat as well as the unburned zones clearly suggest that the thermally-thin assumption, widely used in previous studies, is not valid (see Refs. [18, 20, 28] for example).

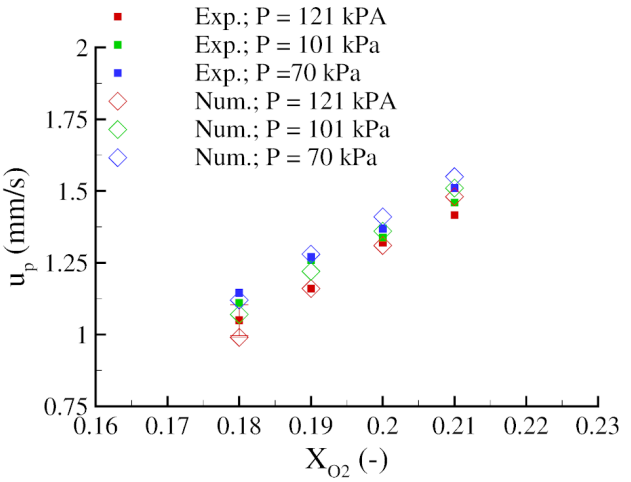

Figure 5. Spread rate as a function of X_{O2} for different pressures. The oxidizer velocity is 150 mm/s and the Type#2 wire is considered.

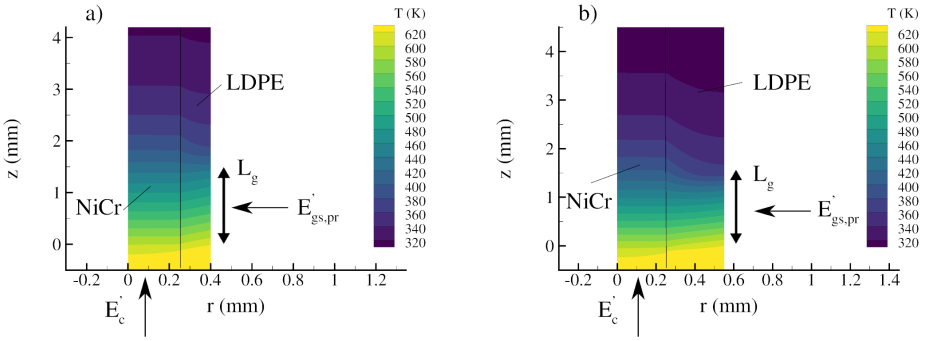

Figure 6. Temperature fields in the wire at steady state for (a) Type#1 and (b) Type#2. In both cases, the oxygen concentration and the pressure are 19 % and 101 kPa, respectively. The axis are not in the same scale.

(2) In the preheat zone, the surface temperature of LDPE is larger than that of NiCr. This behavior is observed for the other conditions. This suggests that, in this case, the heat transfer from the flame dominates in this region.

(3) The metallic core has a significant impact on the temperature field, and, therefore, on the FSR. In order to quantify this effect, simulations have been run by assuming that, on the one hand, the core is also LDPE with a conductivity significantly lower than NiCr ($k_s \approx 0.3 W/m/K$, see Table 2) and, on the other hand, by considering iron (Fe) as the metal. Fe has a conductivity about four times higher than that of NiCr ($k_{Fe} = 58.1 W/m/k$) [19]. Figures 7(b) and (c) show the temperature distribution at steady state for the Type #1 wire in the cases where the core is LDPE and Fe, respectively. A comparison with the temperature distribution for the NiCr Type #1 wire in Figure 6(a) illustrates clearly the role of metallic core and its conductivity. When pure LDPE is considered, the heating beyond the preheat zone ($z > L_g$) is negligible and the FSRs are substantially lower for all wire geometries, as shown in Figures 4 and 7(a). This behavior agrees with previous experimental observations [4]. When Fe is considered, the heating beyond the preheat

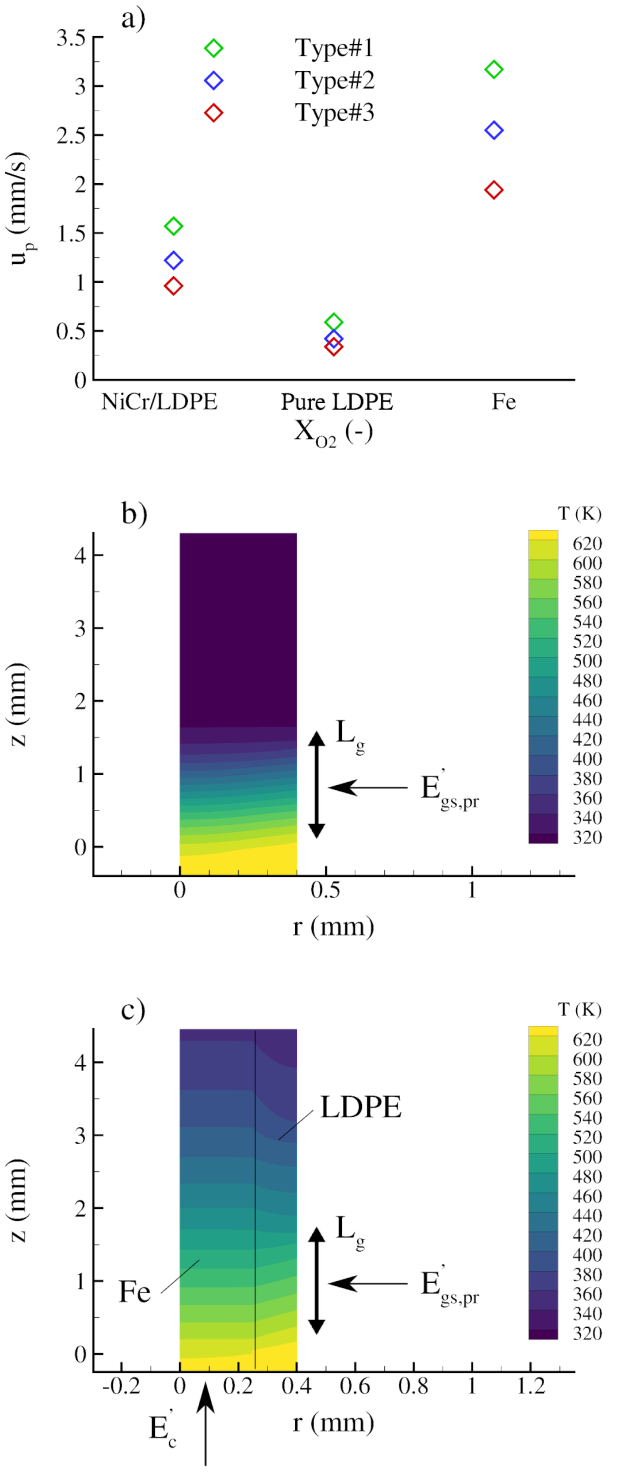

Figure 7. (a) Evaluation of the FSR for NiCr/LDPE and pure LDPE wires. (b) Temperature field for Type #1 pure LDPE wire. (c) Temperature field for Type #1 Fe/LDPE wire. The oxygen concentration and the pressure are 19 % and 101 kPa, respectively.

zone occurs over longer distances than for NiCr, resulting in higher spread rates (see Figure 7(a)).

(4) Let us first consider the effects of the wire geometry the case where the metallic core is made of NiCr. In the preheat zone, particularly at the vicinity of the flame front, temperature gradients observed in Figure 6 show that heat is transferred from the LDPE to the NiCr, i.e., the core acts as a heat sink for both depicted wire geometries. The heat balance in the preheat zone governs the flame extinction process, and this behavior could suggest that the metallic core has a role in this phenomena [28]. An opposite behavior is observed in the unburned zone with the heat being transferred from the metallic core to

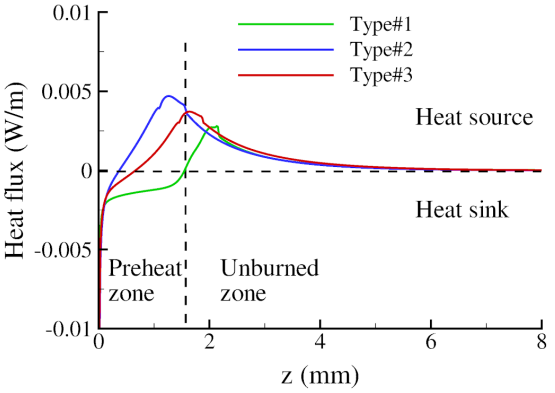

Figure 8. Conductive heat flux between the NiCr core and the LDPE coating, in W/m, in the preheat and unburned zones, for three wire geometries, along the wire length. The oxygen concentration and the pressure are 19 % and 101 kPa, respectively. Positive (negative) heat flux values denote heat transfer from the NiCr (LDPE) to the LDPE (NiCr), i.e., the core acts as a heat source (sink).

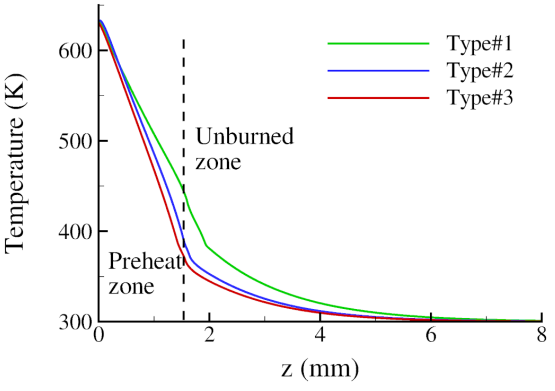

Figure 9. LDPE surface temperature, in *K*, in the preheat and unburned zones for a Nicr metallic core of Type #1. The oxygen concentration and the pressure are 19 % and 101 kPa, respectively.

the LDPE. The metallic core acts then as a heat source in this region, heating the LDPE before the preheat zone. A quantitative analysis of the heat transfer between the NiCr and LDPE along the wire length is shown in Figure 8. The pyrolysis front is at $z = 0$ and both preheat ($0 < z < L_g$) and unburned ($z > L_g$) zones are depicted. This figure illustrates the change of heat transfer direction between the preheat and the unburned zones. It also highlights the role of the LDPE thickness in the heat transfer between the LPDE and NiCr in the preheat zone. It appears that the length over which the NiCr core acts as a sink increases with decreasing LDPE thickness. For the thinner wire (Type #1), it acts as a heat sink over the entire preheat zone while, for the other wires, the length of the heat sink zone reduces. The role of the metallic core on the preheating process is further illustrated in Figure 9 which shows the elevation of LDPE surface temperature ahead of the flame front. The surface temperature increases as the coating thickness is reduced. For the thinner wire (Type #1), the surface temperature at the transition between the unburned and preheat zone exceeds the LDPE melting temperature. Let us investigate further the effects of the conductivity of the metallic core. In the case of pure LPDE, the conductive heat transfer in both r- and z-directions is negligible as indicated by the weak temperature gradients in Figure 7(b). On the other hand, Figure 10 compares the conductive heat transfer between the LDPE and the metallic core for Fe and NiCr for the thinnest Type #1 wire. The heat transfer exhibits a similar trend for both Fe and NiCr, with the core acting as a heat sink in the preheat zone and as a heat source in the unburned zone. However, the heat flux is conducted over a length significantly longer in the preheat zone in the case of Fe. This is confirmed by Figure 11 that shows that the heating process in the preheat zone is much more efficient for the Fe case, leading to a surface temperature of LDPE about about 486 K at the transition between the preheat and unburned zones.

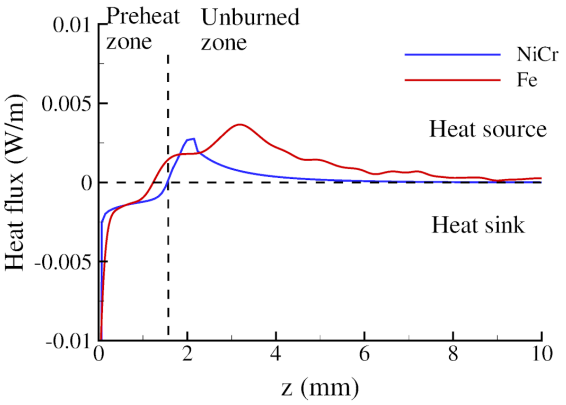

Figure 10. Conductive heat flux between the metallic core (Nicr or Fe) and the LDPE coating, in W/m, in the preheat and unburned zones, for Type #1 wire, along the wire length. The oxygen concentration and the pressure are 19 % and 101 kPa, respectively. Positive (negative) heat flux values denote heat transfer from the metallic core (LDPE) to the LDPE (metallic core), i.e., the core acts as a heat source (sink).

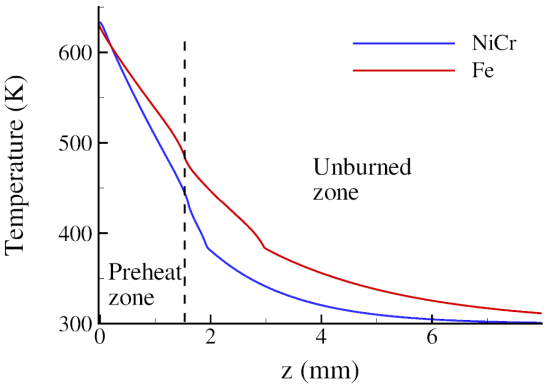

Figure 11. LDPE surface temperature, in K, in the preheat and unburned zones for a metallic core Type #1 made either of NiCr or Fe. The oxygen concentration and the pressure are 19 % and 101 kPa, respectively.

5. Conclusions

An engineering solution for a creeping flame spread model over idealized electrical wires composed of a NiCr metallic core and a LDPE coating in microgravity has been proposed and validated against experimental data obtained in parabolic flights. It has been shown that the heat transfer problem can be simplified by ignoring the heat flux from the bare metallic core and solving the coupled heat transfer equations for LDPE and NiCr in the pyrolysis zone and ahead of the pyrolysis front in conjunction with a simple phase-change based pyrolysis model for LDPE, an Oseen approximation of the flow and a infinitely fast chemistry for gas-phase combustion. The model reduces then to two parameters, the diffusive heat length and the heat conveyed from the flame to a flat surface, this latter depending only on the oxygen concentration in the oxidizer. The first parameters has been estimated from its definition whereas the second has been calibrated to match experimental flame spread rate as a function of the oxygen concentration for given wire geometry and ambient pressure and inflow velocity. The model with the calibrated parameters has been applied successfully to predict flame spread rates for other wire geometries and pressure conditions. A full validation of this model would require more experimental data on wire geometries and natures of the metallic core, which is a main perspective of this work.

The heat transfer mechanisms ahead of the pryolysis front have been investigated. The polymer has been shown to be thermally thick for all tested wire geometries. It has been showed that, in the preheat zone, the contribution of the flame flux dominate the LDPE heating process. In this region the metallic core can act as a heat sink or a heat source depending on the wire geometry. Upstream to the preheat zone, the metallic core behaves as a heat source whatever the wire geometry and the core conductivity. Its contribution to the heating process of the LDPE up to the pyrolysis temperature is enhanced with the core conductivity and as the LPDE thickness decreases.

Nomenclature

A	Cross section area, m^2
B	Mass transfer number
c	Heat capacity, $J/kg/K$
C	Corrective heat transfer factor for a cylindrical geometry
E_{cc}	Heat transferred in the metallic core, W
$E_{gs,pr}$	Heat transferred from the flame to the polymer, W
$E_{gs,pr,flat}$	Heat transferred from the flame to the polymer in a flat slab, W
h_s	Solid enthalpy, J/kg
k	Thermal conductivity, $W/m/K$
L_v	Latent heat of vaporization, J/kg
L_g	Preheat length, m
P	Pressure, Pa
$\dot{q}''_{fl,c}$	Convective heat flux transferred from the flame to the solid, W/m^2
$\dot{q}''_{r,c}$	Radiatiive heat flux transferred from the flame to the solid, W/m^2
$\dot{q}''_{rr}$	Surface re-radiation, W/m^2
r	Radial direction
r_f	Mass-to-fuel ratio
R	Radius, m
t	Time, s
T	Temperature, K
u	Velocity, mm/s
X_{O2}	Oxygen mole fraction
$Y_{O2,\infty}$	Oxygen mass fraction
z	Axial direction

Greek symbols

α	Thermal diffusivity, m^2/s
δ	Insulation thickness, mm
μ	Kinematic viscosity, $Pa.s$
ρ	Density, kg/m^3

Subscripts

c	Metallic core
g	Gas phase
m	Melting
p	Pyrolysis
s	Polymer
∞	Ambient conditions

Superscripts

'	Per meter
"	Per meter squared

Acronyms

FSR	Flame spread rate
LDPE	Low-density polyethylene
NiCr	Nickel-Chrome

Conflicts of interest

The authors declare no competing financial interest.

References

[1] Y. Nakamura, N. Yoshimura, T. Matsumura, H. Ito, O. Fujita, "Flame Spread over Polymer-Insulated Wire in Sub-Atmospheric Pressure: Similarity to Microgravity Phenomena", p. 17-27, Springer, 2008.

[2] L. Hu, Y. Zhang, K. Yoshioka, H. Izumo, O. Fujita, "Flame spread over electric wire with high thermal conductivity metal core at different inclinations", *Proc. Combust. Inst.* **35** (2015), no. 3, p. 2607-2614.

[3] Y. Kobayashi, X. Huang, S. Nakaya, M. Tsue, C. Fernandez-Pello, "Flame spread over horizontal and vertical wires: The role of dripping and core", *Fire Safety Journal* **91** (2017), p. 112-122, Fire Safety Science: Proceedings of the 12th International Symposium.

[4] X. Huang, Y. Nakamura, "A Review of Fundamental Combustion Phenomena in Wire Fires", *Fire Technol.* **56** (2020), p. 315-360.

[5] O. Fujita, M. Kikuchi, K. Ito, K. Nishizawa, "Effective mechanisms to determine flame spread rate over ethylene-tetrafluoroethylene wire insulation: Discussion on dilution gas effect based on temperature measurements", *Proc. Combust. Inst.* **28** (2000), no. 2, p. 2905-2911.

[6] A. Umemura, M. Uchida, T. Hirata, J. Sato, "Physical model analysis of flame spreading along an electrical wire in microgravity", *Proc. Combust. Inst.* **29** (2002), no. 2, p. 2535-2543.

[7] S. Takahashi, H. Takeuchi, H. Ito, Y. Nakamura, O. Fujita, "Study on unsteady molten insulation volume change during flame spreading over wire insulation in microgravity", *Proc. Combust. Inst.* **34** (2013), no. 2, p. 2657-2664.

[8] J.-M. Citerne, H. Dutilleul, K. Kizawa, M. Nagachi, O. Fujita, M. Kikuchi, G. Jomaas, S. Rouvreau, J. L. Torero, G. Legros, "Fire safety in space – Investigating flame spread interaction over wires", *Acta Astronautica* **126** (2016), p. 500-509, Space Flight Safety.

[9] A. Guibaud, J.-M. Citerne, J.-L. Consalvi, G. Legros, "On the effects of opposed flow conditions on non-buoyant flames spreading over polyethylene-coated wires – Part I: Spread rate and soot production", *Combust. Flame* **221** (2020), p. 530-543.

[10] M. Nagachi, F. Mitsui, J.-M. Citerne, H. Dutilleul, A. Guibaud, G. Jomaas, G. Legros, N. Hashimoto, O. Fujita, "Effect of Ignition Condition on the Extinction Limit for Opposed Flame Spread Over Electrical Wires in Microgravity", *Fire Technol.* **56** (2020), p. 149-168.

[11] I. S. Wichman, "Theory of opposed-flow flame spread", *Progress in Energy and Combustion Science* **18** (1992), no. 6, p. 553-593.

[12] R. F. McAlevy, R. S. Magee, "The mechanism of flame spreading over the surface of igniting condensed-phase materials", *Symposium (International) on Combustion* **12** (1969), no. 1, p. 215-227.

[13] F.-P. Carlos, "The solid phase", in *Combustion Fundamentals of Fire*, Academic Press Inc., 1994, p. 31-100.

[14] J. N. De Ris, "Spread of a laminar diffusion flame", *Symposium (International) on Combustion* **12** (1969), no. 1, p. 241-252.

[15] M. A. Delichatsios, "Creeping flame spread: Energy balance and application to practical materials", *Symposium (International) on Combustion* **26** (1996), no. 1, p. 1495-1503.

[16] M. A. Delichatsios, R. A. Altenkirch, M. F. Bundy, S. Bhattacharjee, L. Tang, K. Sacksteder, "Creeping flame spread along fuel cylinders in forced and natural flows and microgravity", *Proc. Combust. Inst.* **28** (2000), no. 2, p. 2835-2842.

[17] M. A. Delichatsios, "Relation of opposed flow (creeping) flame spread with extinction/ignition", *Combust. Flame* **135** (2003), no. 4, p. 441-447.

[18] S. Takahashi, H. Ito, Y. Nakamura, O. Fujita, "Extinction limits of spreading flames over wires in microgravity", *Combust. Flame* **160** (2013), no. 9, p. 1900-1902.

[19] Y. Konno, N. Hashimoto, O. Fujita, "Role of wire core in extinction of opposed flame spread over thin electric wires", *Combust. Flame* **220** (2020), p. 7-15.

[20] Y. Konno, N. Hashimoto, O. Fujita, "Downward flame spreading over electric wire under various oxygen concentrations", *Proc. Combust. Inst.* **37** (2019), no. 3, p. 3817-3824.

[21] A. Guibaud, J. L. Consalvi, J. M. Orlac'h, J.-M. Citerne, G. Legros, "Soot Production and Radiative Heat Transfer in Opposed Flame Spread over a Polyethylene Insulated Wire in Microgravity", *Fire Technol.* **56** (2020), p. 287-314.

[22] A. Guibaud, "Flame spread in microgravity environment : influence of ambient flow conditions", PhD Thesis, Sorbonne University, Paris, France, 2019, Thèse de doctorat dirigée par Legros, Guillaume et Consalvi, Jean-Louis, Mécanique Sorbonne université 2019, http://www.theses.fr/2019sorus129.

[23] A. Guibaud, J.-L. Consalvi, J.-M. Citerne, G. Legros, "Pressure effects on the soot production and radiative heat transfer of non-buoyant laminar diffusion flames spreading in opposed flow over insulated wires", *Combust. Flame* **222** (2020), p. 383-391.

[24] A. Guibaud, J.-M. Citerne, J.-L. Consalvi, O. Fujita, J. L. Torero, G. Legros, "Experimental evaluation of flame radiative feedback: methodology and application to opposed flame spread over coated wires in microgravity", *Fire Technol.* **56** (2020), no. 1, p. 185-207.

[25] J.-L. Consalvi, A. Guibaud, A. Coimbra, J.-M. Citerne, G. Legros, "Effects of oxygen depletion on soot production,

emission and radiative heat transfer in opposed-flow flame spreading over insulated wire in microgravity", *Combust. Flame* **230** (2021), article no. 111447.

[26] M. A. Delichastsios, "Exact Solution for the Rate of Creeping Flame Spread over Thermally Thin Materials", *Combustion Science and Technology* **44** (1986), no. 5-6, p. 257-267.

[27] A. Coimbra, J. Sarazin, S. Bourbigot, G. Legros, J.-L. Consalvi, "A semi-global reaction mechanism for the thermal decomposition of low-density polyethylene blended with ammonium polyphosphate and pentaerythritol", *Fire Safety Journal* **133** (2022), article no. 103649.

[28] Y. Konno, Y. Kobayashi, C. Fernandez-Pello, N. Hashimoto, S. Nakaya, M. Tsue, O. Fujita, "Opposed-Flow Flame Spread and Extinction in Electric Wires: The Effects of Gravity, External Radiant Heat Flux, and Wire Characteristics on Wire Flammability", *Fire Technol.* **56** (2020), p. 131-148.

[29] A. Guibaud, J.-M. Citerne, J.-L. Consalvi, O. Fujita, J. L. Torero, G. Legros, "Experimental Evaluation of Flame Radiative Feedback: Methodology and Application to Opposed Flame Spread Over Coated Wires in Microgravity", *Fire Technol.* **56** (2020), p. 185-207.

[30] Y. Sano, S. Nishikawa, "The Heat Transfer Coefficient of Fine Wires in Air Flow", *Chemical Engineering* **28** (1964), no. 4, p. 275-284.

[31] S. V. Patankar, *Numerical heat transfer and fluid flow*, Series on Computational Methods in Mechanics and Thermal Science, Hemisphere Publishing Corporation, 1980.

[32] J. E. Mark (ed.), *Physical Properties of Polymers Handbook*, second ed., Springer, 2007.

[33] Y. Kobayashi, K. Terashima, M. A. F. bin Borhan, S. Takahashi, "Opposed Flame Spread over Polyethylene Under Variable Flow Velocity and Oxygen Concentration in Microgravity", *Fire Technol.* **56** (2020), p. 113-130.

[34] M. Thomsen, C. Fernandez-Pello, X. Huang, S. Olson, P. Ferkul, "Buoyancy Effect on Downward Flame Spread Over PMMA Cylinders", *Fire Technol.* **56** (2020), no. 1, p. 247-269.